Pergamon

Int. J. Heat Mass Transfer. Vol. 39, No. 11, pp. 2271–2282, 1996

0017-9310/96 $15.00 + 0.00

0017-9310(95)00286-3

Bulk flow pulsations and film cooling—I. Injectant behavior

P. M. LIGRANI, R. GONG and J. M. CUTHRELL

Convective Heat Transfer Laboratory, Department of Mechanical Engineering University of Utah, Salt Lake City, UT 84112, U.S.A.

and

J. S. LEE

Turbo and Power Machinery Research Center, Department of Mechanical Engineering, Seoul National University, Seoul 151-742, Korea

(*Received for publication* 14 *August* 1995)

Abstract—Experimental results are presented which describe the effects of bulk flow pulsations on film cooling from a single row of simple angle film cooling holes. The pulsations are in the form of sinusoidal variations of static pressure and streamwise velocity. Visualizations of film cooling distributions and trajectories illustrate dramatic alterations which occur as the pulsations are imposed on the film cooled boundary layer. In particular, significant changes occur as the coolant Strouhal number becomes greater than 1–2 and the film changes from quasi-steady behavior to non-quasi-steady behavior. Data from these two regimes are presented and discussed along with time-averaged surveys of injectant distributions at different streamwise locations, both with and without pulsations. The results provide clear evidence of the dramatic impact of bulk flow pulsations on film cooling heat transfer. Copyright © 1996 Elsevier Science Ltd.

INTRODUCTION

Turbine unsteadiness develops from four different sources: (i) potential flow interactions, (ii) shock waves, (iii) wake passage, and (iv) random freestream turbulence from the combustion chamber.

Of these, the two having the most dramatic effect on film cooling are potential flow interactions and passing shock waves. This is because both result in important variations of the *static* pressure near turbine surfaces as blade rows move relative to each other. These occur near cooling hole exits as well as in the boundary layers just downstream of the injection holes. As a result, the coolant flow rates pulsate at film hole exits, and injectant trajectories and coverage vary with time downstream of the film holes. Certain low NO_x combustion chambers also produce important static pressure variations in the turbine, however, frequencies are generally less than the pulsations which result from the relative motion of adjacent blade rows.

The changes to film protection produced by passing wakes are significantly less than ones pertaining to shock waves and potential flow disturbances. This is because the static pressure variations produced by wakes are relatively minimal. According to refs. [1–3], high freestream unsteadiness is often more important than passing wakes, and passing wake effects on film cooling and heat transfer are equivalent to mild increases in freestream turbulence intensity. Passing wakes are characterized by periodic *total* pressure pulsations and increased turbulence levels. These sometimes increase diffusion rates which cause the film to spread laterally, so that it becomes somewhat less concentrated as it is advected away from the holes.

Studies which address the effects of wake flows on film cooling are described in refs. [1–5]. Studies which address the influences of passing shock waves and wakes on film cooling are described in refs. [6–8]. Of the important studies of shock waves on turbine heat transfer with no film cooling, Ashworth *et al.* [9], Johnson *et al.* [10], Rigby *et al.* [7], and Abhari *et al.* [11] all measured or predicted massive pulses of surface heat transfer from shock passage relative to heat transfer variations from all other events, including wakes. According to Johnson *et al.* [10], perturbations to local heat transfer rates from the shock waves may be as large as four times the mean levels, with both positive and negative short-duration heat transfer pulses.

The present study is designed to quantify the detailed effects of bulk flow pulsations on film cooling from a single row of simple angle holes. The pulsations are created in the form of sinusoidal variations of *static* pressure and streamwise velocity. The results illustrate dramatic changes to film cooling from this type of pulsating flow, common in all turbines at subsonic speeds from potential flow interactions and at transonic speeds from passing shock waves and potential flow interactions. New understanding of the physical interactions between pulsations and film cooling is thus provided, thereby enabling the development of

NOMENCLATURE

d	injection hole diameter
l	injection hole length
m	instantaneous blowing ratio $\rho_c u_c/\rho_\infty \bar{u}_\infty$
$\overline{m}$	time-averaged blowing ratio $\rho_c \bar{u}_c/\rho_\infty \bar{u}_\infty$
n	pulsation frequency [Hz]
t	temperature, time
St_c	coolant Strouhal number, $2\pi nl/\bar{u}_c$
St_∞	freestream Strouhal number, $2\pi n\delta/\bar{u}_\infty$
u	velocity
x	streamwise distance measured from downstream edge of injection holes
X	streamwise distance measured from trip
y	distance normal to the surface
z	spanwise distance from test surface centerline.

Greek symbols

δ	boundary layer thickness
ρ	density
τ	time period of one pulsation
ν	kinematic viscosity.

Subscripts

c	injectant at exit plane of injection holes
cc	injectant hole centerline value at exit plane of injection holes
o	stagnation condition
r	recovery condition
∞	freestream.

Superscripts

$\bar{}$	time-average.

improved design techniques and improved numerical models to account for these effects. No similar study on pulsations and film cooling is presently known to the authors.

EXPERIMENTAL APPARATUS AND PROCEDURES

The experiment is conducted on a large scale to allow detailed probing of flow features. Low speeds, flat plate test sections, and constant property flows are used to isolate the interactions between the film cooling, imposed bulk flow pulsations and boundary layer.

Wind tunnel

The wind tunnel is open-circuit, subsonic, and located in the Convective Heat Transfer Laboratory of the Department of Mechanical Engineering of the University of Utah. A centrifugal blower is located at the upstream end, followed by a diffuser, a header containing a honeycomb and three screens, and then a 16 to 1 contraction ratio nozzle. The nozzle leads to the test section which is a rectangular duct 3.05 m long and 0.61 m wide, with a top wall having adjustable height to permit changes in the streamwise pressure gradient. The zero pressure gradient employed here is set to within 0.001 in of water differential pressure along the length of the test section, both with and without pulsations. Flow at the test section inlet shows excellent spatial uniformity and a freestream turbulence level less than 0.1% at a freestream velocity of 10 m s^{-1}.

A schematic of the test section, including the coordinate system and apparatus used for flow visualization, is shown in Fig. 1. A boundary layer trip is located on the test plate just downstream of the nozzle exit. The downstream edge of the injection holes is then 1.050 m downstream of the trip, and measuring stations are subsequently located at x/d of 4.5, 9.8, 16.4 and 24.1. Corresponding Reynolds numbers, based on streamwise distance (from the trip) and a freestream velocity of 1.0 m s^{-1}, range from 74 000 to 102 000. For a freestream velocity of 2.0 m s^{-1}, the same Reynolds number ranges from 148 000 to 204 000.

Film cooling configuration and air supply

The film cooling holes are placed in a single row with spanwise spacing of three hole diameters. Each hole is oriented in a streamwise/normal plane (i.e. with a simple angle orientation) at a 35° angle from the test surface. Hole diameter is 2.22 cm, giving an l/d ratio of 4.0, and δ/d of 1.53 at $x/d = 4.5$ at a freestream velocity of 2.0 m s^{-1}. Ratios of displacement thickness to hole diameter, and momentum thickness to hole diameter at the same u_∞ are 0.224, and 0.155, respectively. Blowing ratio $\bar{m}$ ranges from 0.10 to 0.59. The ratio of injectant to freestream density ρ_c/ρ_∞ is 1.0 for all flow visualization tests and approximately 0.90 for the injectant surveys. Injection Reynolds number $d\bar{u}_c/\nu$ then ranges from 720 to 850 for most cases investigated. Ridged tips, placed around the interior circumference of each injection hole, are used to maintain turbulent injectant. Turbulent flow at the injection hole exits is confirmed from measurements of instantaneous velocity made using hot-wire probes.

The air used for the film first flows through a regulating valve, followed by a moisture trap, rotometer, diffuser, and finally into the injection heat exchanger and plenum chamber. The regulating valve and roto-

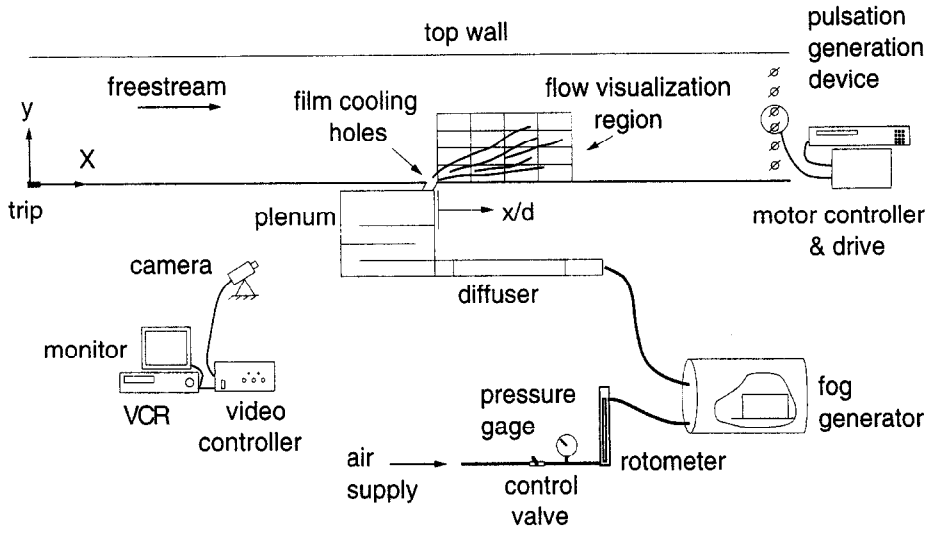

Fig. 1. Schematic of test section and coordinate system including flow visualization equipment.

meter provide means to control the film cooling blowing ratio, and the injection chamber provides means to heat the injectant above ambient temperature.

Visualization of injectant distributions

To track the injectant and determine its distribution along and above the test surface, the injectant air is contaminated with fog. This is accomplished by pressurizing a 50 gallon steel drum housing a theatrical fog generator (Rosco model 1500), as shown in Fig. 1. Fog is produced from the vaporization of a water soluble liquid with this device, and subsequently fed into the diffuser of the injectant air supply system. The air is then photographed against a black background with white grid lines as, and after, it is ejected from the holes. A Mitsubishi CCD72 camera, lens system, control box, HR1000 monitor, and AG-1960 video recorder are used. Individual video images are digitized using Apple Video System software, and then processed and enhanced using Adobe Photoshop image processing software on a Macintosh Performa 636 computer. With this approach, time-resolved injectant distributions, such as the ones in Figs. 6, 9, and 12, are obtained.

Time-averaged injectant distributions

Copper-constantan thermocouples are used to measure temperatures which are correlated to injection distributions. For the distributions, a thermocouple is traversed over spanwise/normal planes using an automated computer-controlled two-dimensional traversing system which may be placed at different streamwise locations. With this traverse, the thermocouple probe is traversed over 10.2 by 20.3 cm spanwise/normal planes at 800 locations spaced 0.51 cm apart in each direction. As the boundary layer is probed at each measurement location, simultaneous measurements are made of the injectant temperature (at hole exits), and freestream temperature. Voltages from thermocouples are digitally sampled and read using Hewlett-Packard 44422 relay multiplexer cards for type T thermocouples, and a Hewlett-Packard 3497A Data Acquisition Control Unit with a 3498A Extender. These units are controlled and resulting data are processed using a Hewlett-Packard model A2240B type 362 mainframe computer.

GENERATION OF BULK FLOW PULSATIONS

Static pressure pulsations are produced in the test section using an array of rotating shutters located at the exit of the test section and driven by a system of gears and an electric motor [12], as shown in Fig. 1. This approach is used because: (1) the shutters oscillate the static pressure without significant total pressure variations [12, 13]; (2) static pressure pulsations produce the most important disruptions to the flow rates, trajectories, and distributions of the film coolant; (3) much higher frequencies of pulsation can be produced than with many other methods [13]; and (4) deterministic sinusoidal variations of static pressure can be produced at selected frequencies [12].

In producing these bulk flow pulsations, two different time scales are important to consider. The first pertains to the time required for the boundary layer to recover fully after the passing of each different type of disturbance [14]. This is characterized by freestream Strouhal number $St_\infty = 2\pi n\delta/\bar{u}_\infty$ which ranges from 0.31 to 2.40 in the present study. The second important time scale pertains to the adjustment of coolant flow rates. Temporal pressure variations will influence the coolant mass flow rate when the disturbance passing frequency is low, compared with the time required for the flow to pass through the coolant holes [8]. This occurs if the product of coolant flow Mach number M_c and coolant Strouhal number $St_c = 2\pi nl/\bar{u}_c$ is about 1

or less ($M_c St_c \leqslant 1$) [8]. Typical values for operating turbines range from 0.2 to 0.6, which gives St_c from 0.2 to 6.0. In the present experiment, St_c is varied from 0.36 to 8.12.

EXPERIMENTAL RESULTS: NO PULSATIONS

Images of the side views of the injectant (viewed in the negative z direction) obtained without pulsations are presented in Figs. 2 and 3. In these two figures, as well as in Figs. 6, 9, and 12, the higher concentrations of the film are evidenced by darker regions. This was accomplished by videotaping the ordinarily white illuminated fog against a black background and white grid lines. Afterwards, the *negative* image of each photograph is produced and then digitally enhanced using the image processing software described earlier. Horizontal spacing between vertical grid lines in the five figures is 1 hole diameter, and vertical spacing between horizontal grid lines is 1/2 hole diameter, as shown in Fig. 2. The test surface is located along the bottom surface of each image in Figs. 2, 3, 6, 9 and 12, and the downstream edge of the film cooling holes is positioned at the first vertical grid line on the left edge of each image.

The results in Fig. 2 show the distribution of film when it is injected into a turbulent boundary layer with no pulsations at $m = 0.32$. Because dark regions persist near the test surface, injectant is abundant near $y = 0$ as it maintains its protection for some distance downstream of the cooling holes. The lighter patterns located near the test surface at $x/d = 5$–7 result partially because the injectant becomes more diffuse as it advects downstream, but mostly because of reduced injectant illumination at these locations.

The image presented in Fig. 3 illustrates film behavior with no imposed pulsations when blowing ratio m is 0.55. In contrast to the results in the previous figure, the most important injectant concentrations are lifting off the surface as x/d increases from 0.5 to 7.

Results illustrating time-averaged injectant distributions in spanwise/normal planes at different streamwise locations are presented in Fig. 4. Such injectant distributions are obtained using techniques developed by Ligrani *et al.* [15, 16] in which the injectant is heated as all other components in the wind tunnel test section are maintained at the freestream (or ambient) temperature. With this approach, the injectant is the only source of thermal energy relative to the freestream flow. Higher magnitudes of $(\bar{t}_r - t_{r\infty})/(t_{rcc} - t_{r\infty})$ then indicate greater concentrations of injectant, and clear indications of the protection (or lack of protection) provided by the injectant to the time-averaged flow field are provided. Near wall values of $(\bar{t}_r - t_{r\infty})/(t_{rcc} - t_{r\infty})$ are particularly important in this regard because they approach magnitudes of the adiabatic film cooling effectiveness [17]. Distributions of $(\bar{t}_r - t_{r\infty})/(t_{rcc} - t_{r\infty})$ such as the ones in Fig. 4 (and Figs. 7 and 10) thus show how injectant accumulates and is rearranged in the boundary layer as a result of advective and diffusive processes.

The results in Fig. 4, obtained with no imposed pulsations and $m = 0.25$, show the highest injectant accumulations just downstream of the holes at $x/d = 4.5$. Here, each concentration is roughly circular or oval in shape, and located near the wall just after the injectant exits the holes. As x/d increases to 9.8, 16.4 and 24.1, the highest injectant concentrations continue to be located near the surface at spanwise

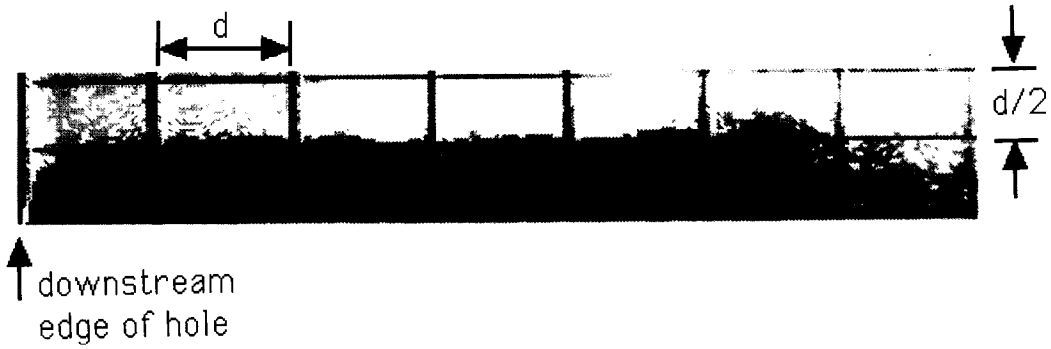

Fig. 2. Side view of injectant distribution obtained with no pulsations $u_\infty = 1.0$ m s^{-1}, and $m = 0.32$.

Fig. 3. Side view of injectant distribution obtained with no pulsations, $u_\infty = 1.0$ m s^{-1} and $m = 0.55$.

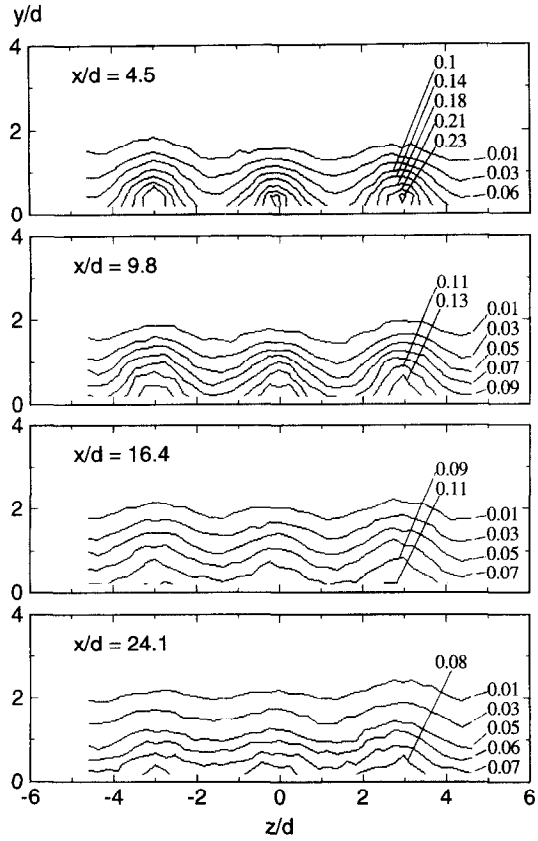

Fig. 4. Surveys of $(\bar{t}_r - t_{r\infty})/(t_{rcc} - t_{r\infty})$ illustrating time-averaged injectant distributions with no pulsations, $u_\infty = 2.0$ m s^{-1} and $m = 0.25$.

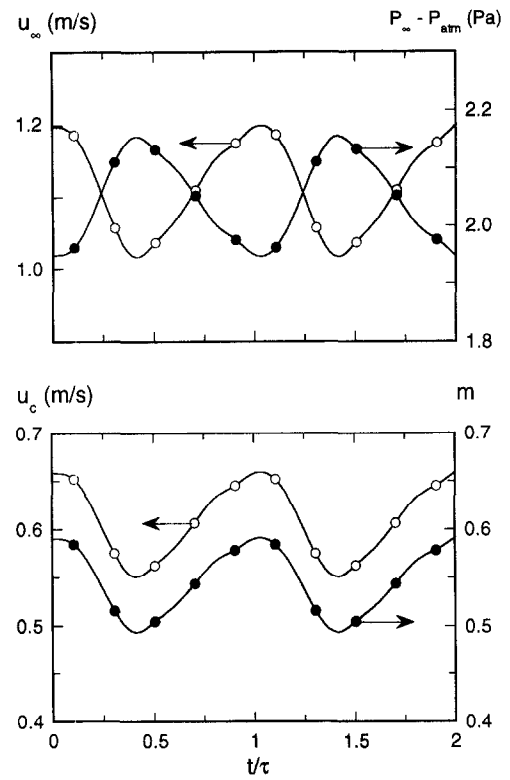

Fig. 5. Time variation of freestream velocity, freestream static pressure, injectant velocity, and injectant blowing ratio obtained with $n = 0.6$ Hz pulsations, $u_\infty = 1.11$ m s^{-1}, $\overline{m} = 0.54$ and $St_c = 0.56$. Time period of one pulsation τ is 1.667 s.

locations downstream of individual holes at z/d of -3, 0 and 3. As for the flow visualization results presented in Fig. 2, the results in Fig. 4 do not evidence significant film lift-off since the largest injectant accumulations are located near the test surface at all x/d.

EXPERIMENTAL RESULTS: QUASI-STEADY FILM BEHAVIOR

Two distinctly different regimes of film cooling behavior with pulsations were discovered from the injectant visualizations: (i) quasi-steady; and (ii) non-quasi-steady. Of these, quasi-steady behavior is now discussed.

Typical variations of freestream static pressure P_∞, freestream velocity u_∞, instantaneous blowing ratio m, and instantaneous injectant velocity u_c (averaged over the hole cross-section) for two pulsation cycles with quasi-steady film behavior are presented in Fig. 5. Variations of freestream static pressure P_∞ are related to variations of freestream velocity u_∞ by the Euler equation for inviscid unsteady flow along a streamline, given by

$$\partial u_\infty/\partial t + u_\infty(\partial u_\infty/\partial x) = -1/\rho(\partial P_\infty/\partial x). \quad (1)$$

With bulk flow pulsations imposed at a frequency of n of 0.6 Hz, the freestream Strouhal number St_∞ is 0.094. This results in quasi-steady flow conditions in the *freestream* [18] and the $\partial u_\infty/\partial t$ term in equation (1) is negligible. Consequently, the relationships between freestream velocity, instantaneous injectant velocity, and freestream static pressure are given by

$$P_{o\infty}/\rho = P_\infty/\rho + u_\infty^2/2$$

$$\text{and} \quad u_c = C_D[2(P_{oc} - P_\infty)/\rho]^{1/2} \quad (2,3)$$

where C_D is the injection hole discharge coefficient.

The trace of freestream velocity u_∞ in Fig. 5 is determined from hot-wire anemometry measurements [18]. Variations of P_∞ and u_c are then calculated using this u_∞ variation in equations (2) and (3) with measured values of freestream total pressure $P_{o\infty}$ and injection plenum total pressure P_{oc}, both of which are nearly constant. With an average freestream velocity of 1.11 m s^{-1}, Fig. 5 shows that the 0.6 Hz pulsating freestream velocity ranges from 1.02 to 1.20 m s^{-1}. This results in a $\pm 9\%$ change both to the injectant velocity and blowing ratio with respect to time-averaged values ($\overline{m} = 0.54$, $\bar{u}_c = 0.60$ m s^{-1}), such that m varies from 0.49 to 0.59. This variation is confirmed by hot-wire anemometry measurements made near the exits of the film cooling holes, which also give u_c which vary by $\pm 9\%$ with respect to $\bar{u}_c$. This agreement also

validates the calculated variation of P_∞ as well as the assumption of quasi-steady *freestream* flow behavior.

Figure 6 shows a sequence of visualized images which illustrate quasi-steady injectant behavior. Here, pulsations are imposed at 0.2 Hz, $St_c = 0.36$ and $\overline{m} = 0.31$. As for Figs 2 and 3, the injectant is viewed from the side in the negative z direction. Distributions are shown at different instants of time in Fig. 6, where time increases from 0.003 τ to 1.00 τ as one's view proceeds down the figure. As this occurs, the entire injectant trajectory oscillates so that it lifts off the test surface and then returns again as time increases during each pulsation. As a result, the continuously varying instantaneous distributions in Fig. 6 are considerably different from the injection distribution shown in Fig. 2, obtained with no pulsations at the same blowing ratio. The film behavior illustrated by Fig. 6 is quasi-steady because the injectant distribution at each instant of time is the same as the steady distribution which would exist at the same instantaneous flow condition. On a turbine surface, such behavior is important because it can cause the injectant to periodically lift-off the surface, thereby decreasing the time-averaged film effectiveness and time-averaged protection compared to a non-pulsating flow.

These characteristics are present because the imposed pulsations produce periodically unsteady static pressure fields at the exits of the injection holes which result in pulsating coolant flow rates. In addition, the pulsating static pressure and velocity

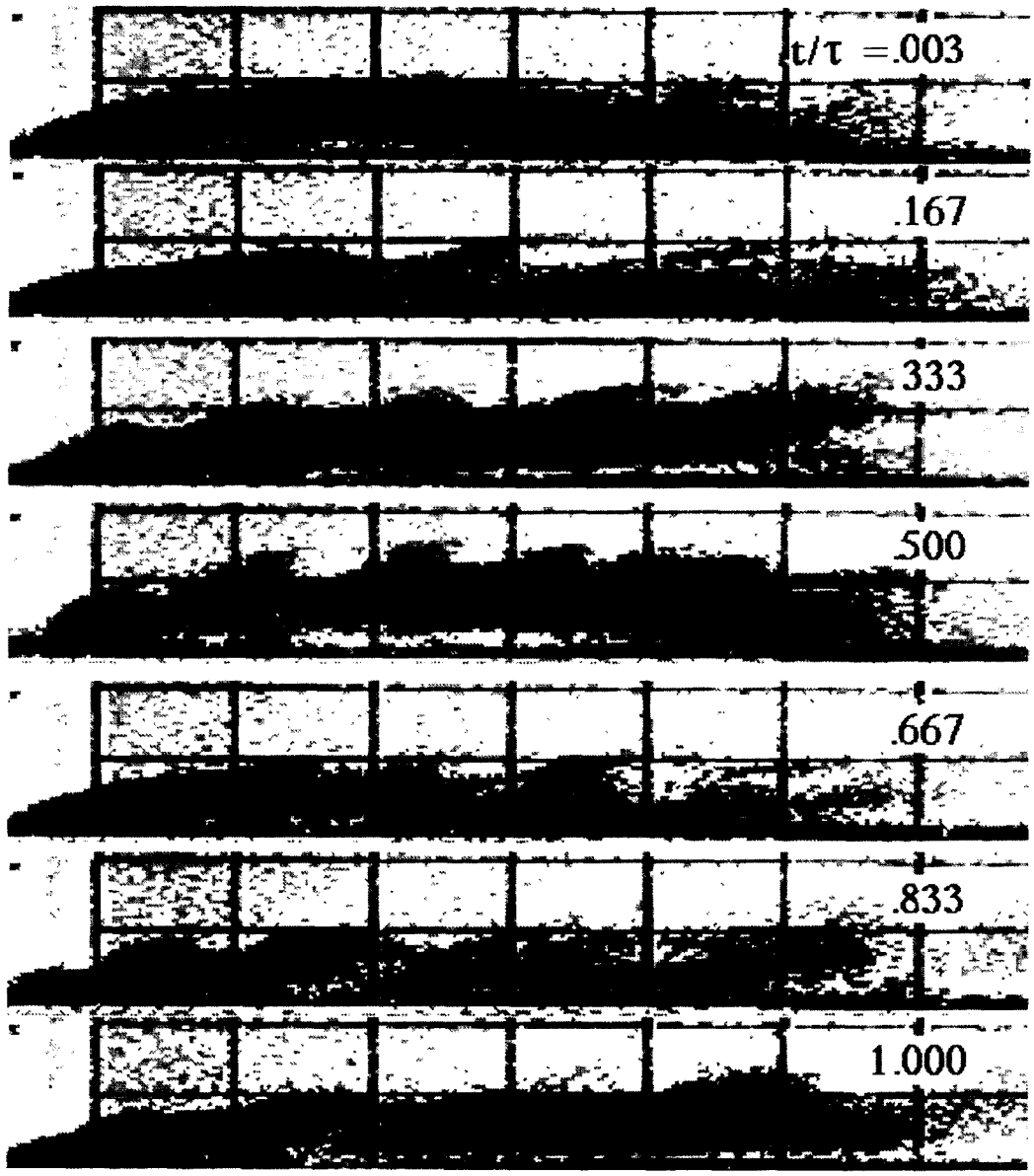

Fig. 6. Side view of injectant distribution at different times obtained with $n = 0.2$ Hz pulsations, $u_\infty = 1.0$ m s^{-1}, $\overline{m} = 0.31$ and $St_c = 0.36$. Time period of one pulsation τ is 5 s.

fields in the boundary layer just downstream from the injection holes result in complex variations with time of the trajectories, distributions, as well as the coverage of the injectant along the surface. The film thus instantaneously changes its momentum and position in the boundary layer over each pulsation period as the bulk flow pulsations are imposed. The mean injectant trajectory with pulsations is also somewhat different, and the same amount of injectant is spread over a larger volume compared to non-pulsating flow.

Surveys which illustrate such time-averaged injectant distributions and behavior under quasi-steady conditions are presented in Fig. 7 for $St_c = 0.67$. Even though there are many qualitative similarities compared to the results obtained with no pulsations in Fig. 4, there are also some quantitative differences. In particular, the $(\bar{t}_r - t_{r\infty})/(t_{rcc} - t_{r\infty})$ distributions in Fig. 7 are slightly more spread out than the distributions in Fig. 4. In addition, regions with the highest injectant concentrations are spread over smaller portions of spanwise/normal planes at all four x/d. Such behavior results because the pulsations act to move the injectant to and from the wall over each pulsation period, thereby spreading a similar quantity of injectant over a larger volume.

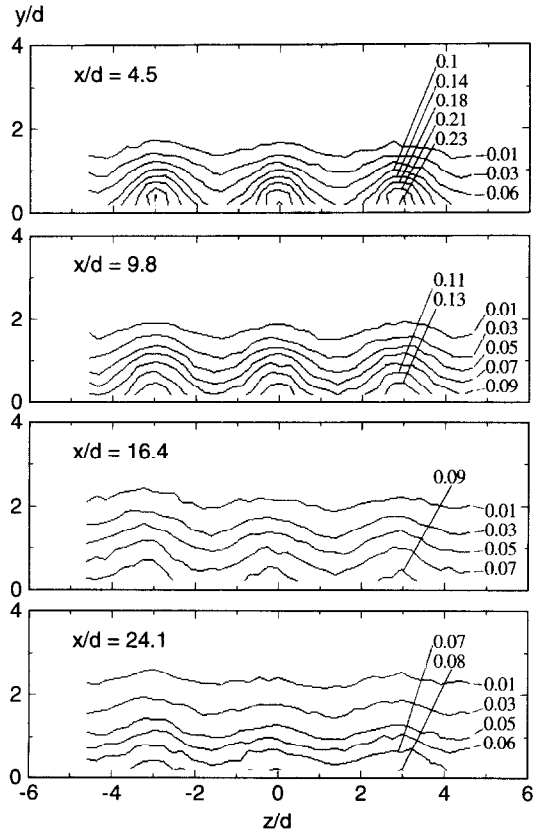

Fig. 7. Surveys of $(\bar{t}_r - t_{r\infty})/(t_{rcc} - t_{r\infty})$ illustrating time-averaged injectant distributions with $n = 0.6$ Hz pulsations, $u_\infty = 2.0$ m s^{-1}, $\bar{m} = 0.25$ and $St_c = 0.67$.

EXPERIMENTAL RESULTS: NON-QUASI-STEADY FILM BEHAVIOR

Nominal non-quasi-steady behavior

Figure 8 shows typical variations of P_∞, u_∞, m and u_c for two pulsation cycles with non-quasi-steady film behavior. Here, $St_c = 7.73$, $\bar{m} = 0.55$, $u_\infty = 1.05$ m s^{-1}, and the time period of one pulsation τ is 0.125 s. The pulsation frequency is 8.0 Hz giving a freestream Strouhal number St_∞ of 2.40. Because n and St_c are so high, the *freestream* is not quasi-steady [18] and the $\partial u_\infty/\partial t$ term in equation (1) is included as freestream static pressure P_∞ is determined from measured variations of freestream velocity u_∞. The resulting static pressure variations at the exit of the film cooling holes cause the instantaneous blowing ratio m to vary $\pm 27\%$ with respect to the mean value $\bar{m} = 0.55$.

Figure 9 shows film distributions which illustrate non-quasi-steady film behavior. Blowing ratio $\bar{m}$ is 0.55 as pulsations are imposed at 8 Hz, which gives a coolant Strouhal number, St_c, of 8.12. Time increases from 0.143 τ to 1.067 τ as one moves down the figure. In this sequence, the whole injectant trajectory is lifted off the test surface. Now, instead of the entire injectant trajectory oscillating in one continuous stream, portions of the film oscillate in ways different from adjacent portions giving a 'wavy' appearance at each

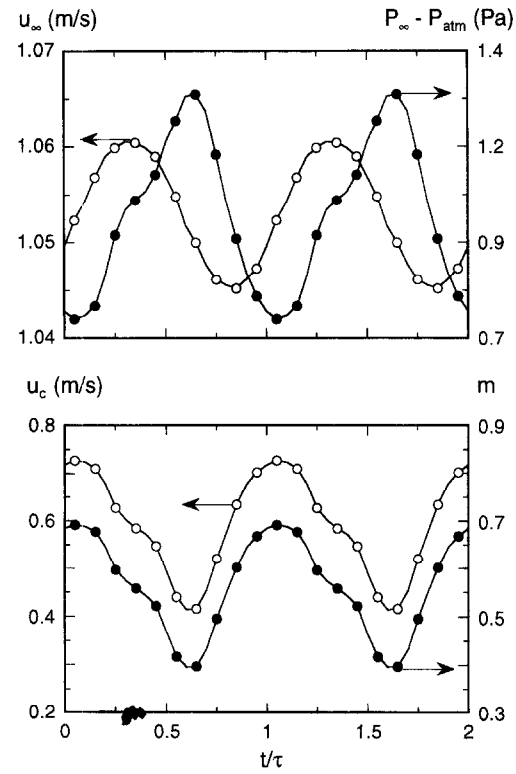

Fig. 8. Time variation of freestream velocity, freestream static pressure, injectant velocity, and injectant blowing ratio obtained with $n = 8.0$ Hz pulsations, $u_\infty = 1.05$ m s^{-1}, $\bar{m} = 0.55$ and $St_c = 7.73$. Time period of one pulsation τ is 0.125 s.

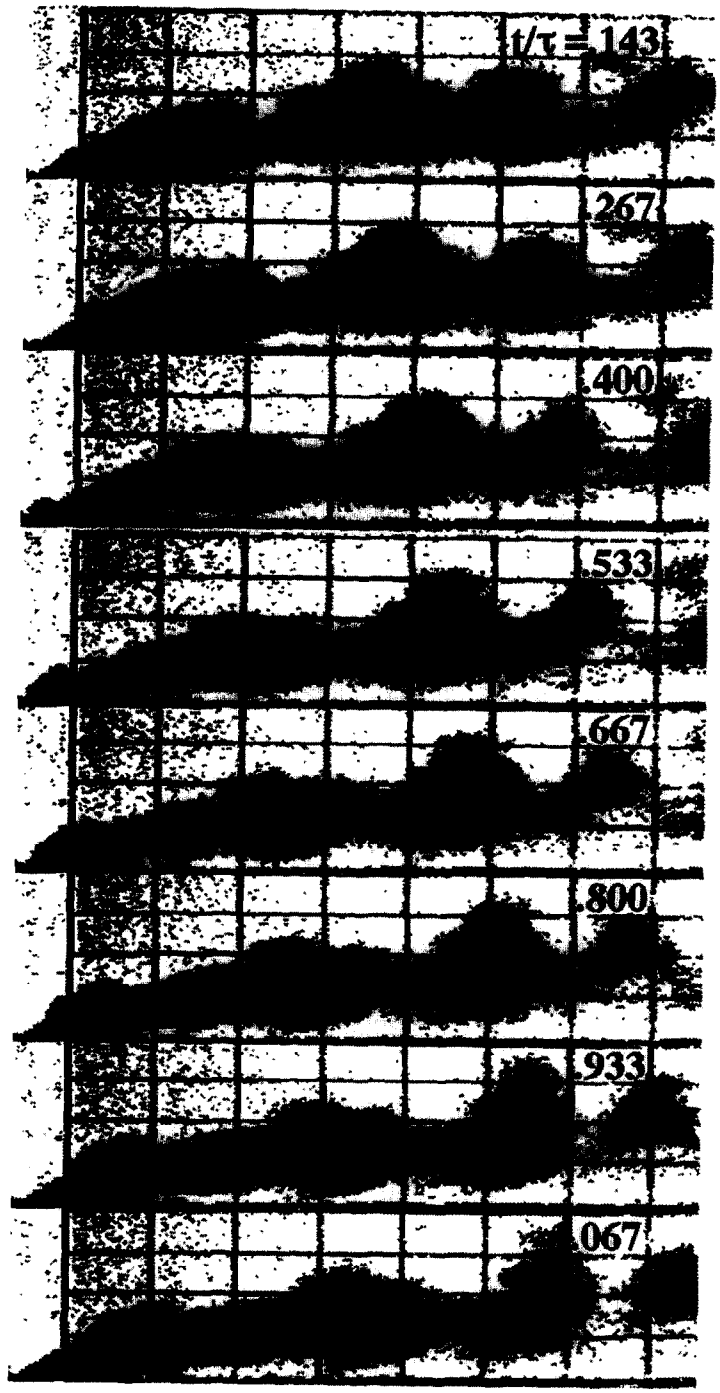

Fig. 9. Side view of injectant distributions at different times obtained with $n = 8.0$ Hz pulsations, $u_\infty = 1.0$ m s^{-1}, $\overline{m} = 0.55$ and $St_c = 8.12$. Time period of one pulsation τ is 0.125 s.

instant in time. With such non-quasi-steady behavior, the spacings between larger accumulations of injectant correspond exactly to the distance that the film moves over one pulsation cycle. Because of these complex variations, the images in Fig. 9 are considerably different from the image presented in Fig. 3 obtained with no pulsations at the same time-averaged blowing ratio. Differences between Figs. 6 and 9 are due, in part, to different phase shifts between instantaneous u_c and instantaneous u_∞. These play an important role here because they generally increase with pulsation frequency.

The 'wavy' fog patterns in Fig. 9 are present because the coolant Strouhal number St_c is greater than 1–2. The coolant Strouhal number represents the ratio of time required for the film to enter and leave an injec-

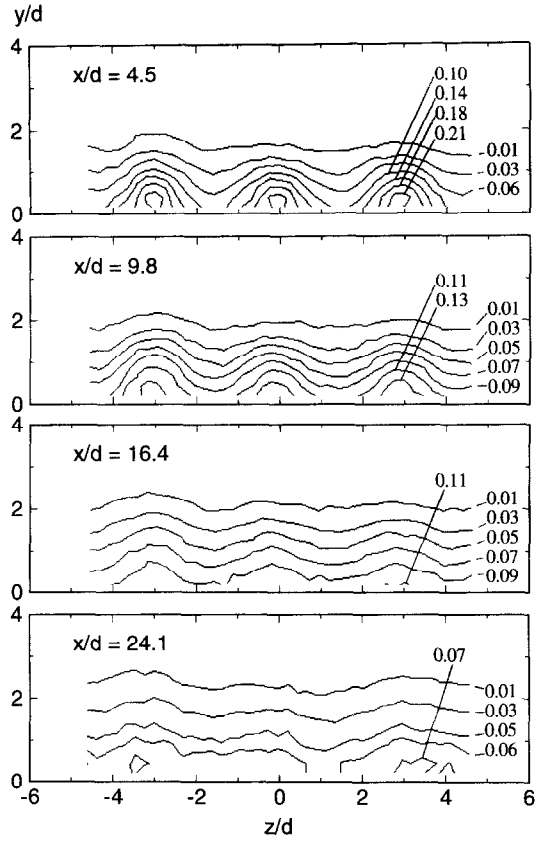

Fig. 10. Surveys of $(\bar{t}_r - t_{r\infty})/(t_{rcc} - t_{r\infty})$ illustrating time-averaged injectant distributions with $n = 8.0$ Hz pulsations, $u_\infty = 2.0$ m s^{-1}, $\overline{m} = 0.25$ and $St_c = 8.93$.

tion hole ($l/\bar{u}_c$) to the time period of one pulsation ($1/2\pi n$). $St_c > 1$–2 thus means that a small parcel of injectant flow is affected by more than one pulsation during the time it enters and leaves the injection hole. As a result, the quantity of injectant from the hole periodically changes over one $l/\bar{u}_c$ time period. Larger amounts (relative to the time-averaged injectant mass flux) emerge when the static pressure at the hole exits is low and the instantaneous blowing ratio m is high. Relatively smaller amounts emerge when the static pressure at the hole exits is high and the instantaneous blowing ratio m is low. Larger amounts then result in the large blobs of injectant shown in Fig. 9, and smaller amounts result in the smaller blobs, resulting in the 'wavy' appearance in each instantaneous injectant visualization.

Surveys of $(\bar{t}_r - t_{r\infty})/(t_{rcc} - t_{r\infty})$ showing time-averaged injectant distributions are presented in Fig. 10 for $St_c = 8.93$. Because of the dramatic alterations resulting from the non-quasi-steady film behavior, distributions in Fig. 10 are less concentrated and more spread out compared to the non-pulsating surveys presented in Fig. 4 and the quasi-steady surveys presented in Fig. 7. Differences are evident at all four x/d investigated (4.5, 9.8, 16.4 and 24), particularly at locations just downstream of the holes and at locations close to the test surface.

Reversing film behavior

Abhari and Epstein [8] point out that reversal of the coolant flow over part of the unsteadiness cycle can occur if the pressure difference between the coolant plenum and the wall *static* pressure at the hole exits is periodically negative. This situation is set-up in the present study at the experimental conditions illustrated in Fig. 11. Here, instantaneous freestream static pressure becomes larger than the time-averaged injection plenum total pressure once each pulsation cycle. As this occurs, the injectant reverses into the plenum altering P_{oc} from its time-averaged magnitude. Plenum total pressure thus varies periodically with each pulsation. The low blowing ratio employed to obtain this result ($\overline{m} = 0.1$) gives an injection Reynolds number $d\bar{u}_c/\nu$ of 140. As a result, the film is probably laminar near the hole exits in spite of the trips placed near the inlet of each film hole. The resulting flow visualization sequence in Fig. 12 shows injectant distributions tremendously different from the ones given in Figs 2, 3, 6 and 9. As time proceeds through one pulsation cycle, complete absence of the injectant is evident just downstream of the hole at $t = 0.007\ \tau$ and $1.000\ \tau$ due to injectant reversal. A large quantity of injectant is then apparent just afterwards as the injectant resumes flowing out of the holes. Such behavior indicates that the surface just downstream of the injection holes has zero film effectiveness and zero protection once each pulsation cycle.

REGIMES OF UNSTEADY FILM BEHAVIOR

A map illustrating different regimes of pulsating film cooling behavior is shown in Fig. 13. Each data point represents the experimental conditions at which injectant distributions were visualized and video taped. From this figure, it is evident that the existence of quasi-steady and non-quasi-steady film behavior with pulsations depends on the magnitude of the coolant Strouhal number, St_c. St_c magnitudes less than 1–

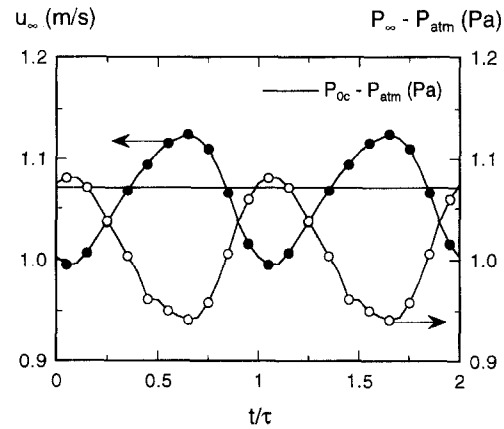

Fig. 11. Time variation of freestream velocity and freestream static pressure obtained with $n = 0.4$ Hz pulsations, $u_\infty = 1.06$ m s^{-1}, $\overline{m} = 0.1$ and $St_c = 2.11$. Time period of one pulsation τ is 2.50 s.

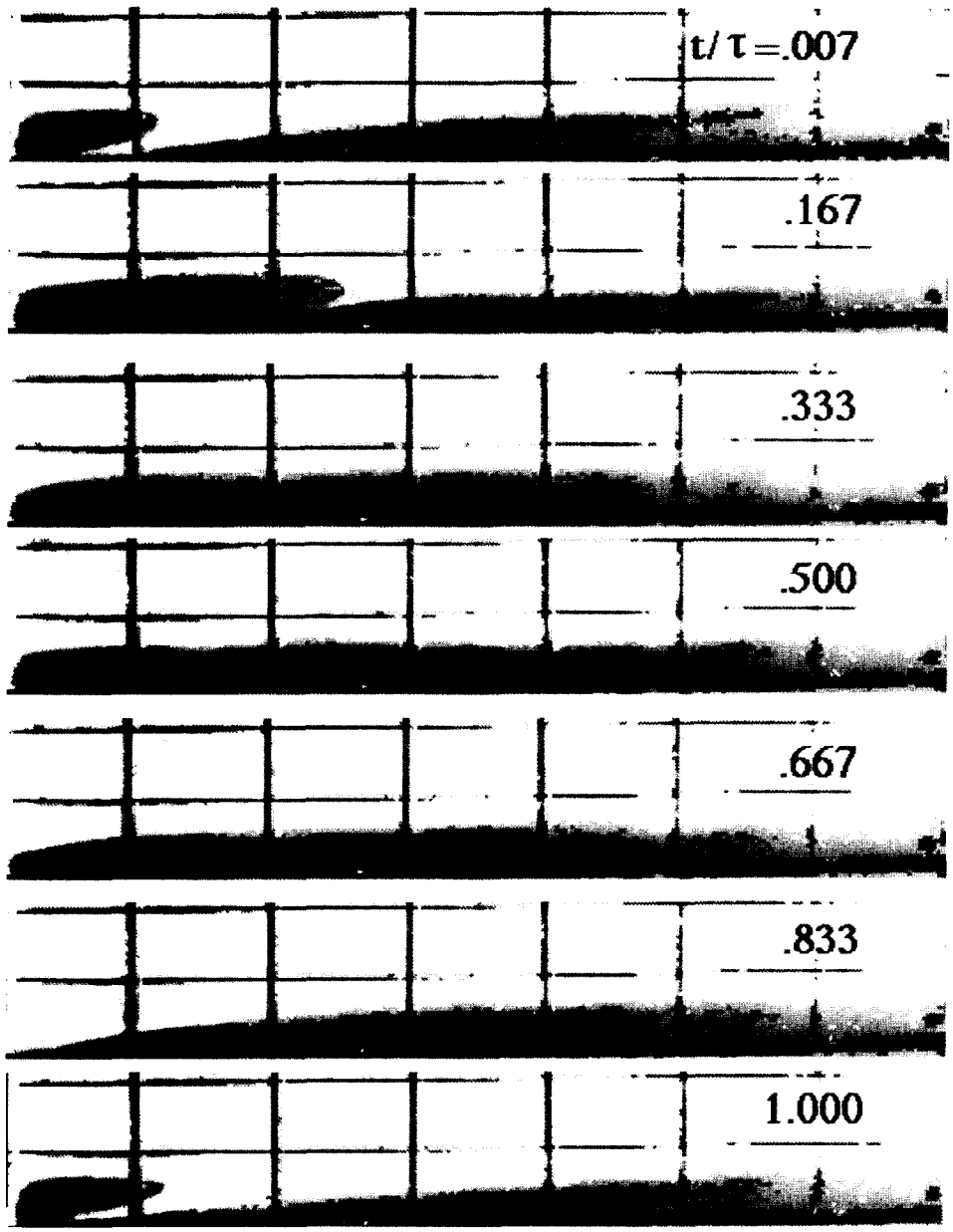

Fig. 12. Side view of injectant distributions at different times obtained with $n = 0.4$ Hz pulsations, $u_\infty = 1.0$ m s^{-1}, $\overline{m} = 0.10$ and $St_c = 2.23$. Time period of one pulsation τ is 2.50 s.

2 correspond to quasi-steady behavior, and St_c magnitudes greater than 1–2 correspond to non-quasi-steady behavior, regardless of the magnitude of the blowing ratio $\overline{m}$.

Conditions for reversing film behavior are also indicated in Fig. 13. With the present experimental set-up, this occurs at blowing ratios in the vicinity of 0.1 or less, at St_c less than 10–20.

SUMMARY AND CONCLUSIONS

The effects of bulk flow pulsations on film cooling with a single row of simple angle film cooling holes is investigated. The pulsations are in the form of near-sinusoidal velocity and static pressure wave forms at frequencies from 0.2 to 8 Hz, which correspond to coolant Strouhal numbers from 0.36 to 8.12. They are produced using an array of rotating shutters placed at the downstream end of the wind tunnel test section. The sinusoidal form for the wave form is chosen because it is easily described and deterministic. Pulsations of static pressure are employed because: (i) they result in significant periodic variations of film cooling flow rates, coverage, and trajectories; and (ii) they occur near turbine surfaces in operating engines from potential flow interactions at subsonic speeds, and from passing shock waves and potential flow interactions at transonic speeds.

The pulsations produce important changes to the flow structure, especially because the imposed pul-

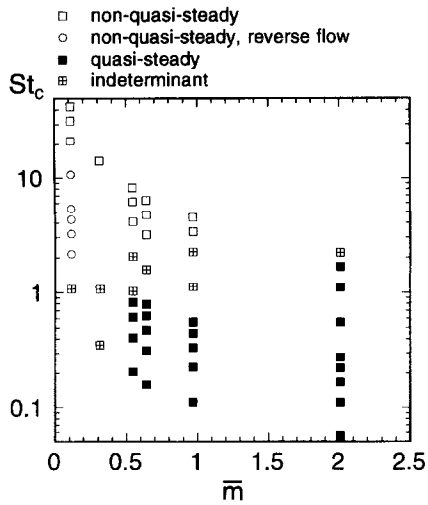

Fig. 13. Map illustrating different regimes of pulsating film cooling behavior.

sations produce periodically unsteady static pressure fields at the exits of the injection holes which result in pulsating coolant flow rates. In addition, the pulsating static pressure and velocity fields in the boundary layer just downstream from the injection holes result in complex variations with time of the trajectories, distributions, as well as the coverage of the injectant along the surface. The film thus instantaneously changes its momentum and position in the boundary layer over each pulsation period as the bulk flow pulsations are imposed. Film concentrations move to and from the wall which often gives a different mean injectant trajectory, and acts to spread the same amount of injectant over a larger volume. As a result, important changes to *time-averaged* injectant distributions occur which are evidenced by surveys of normalized boundary layer recovery temperature. These then evidence important changes to film cooling protection [17].

Two distinctly different regimes of film cooling behavior with pulsations are evident in the time-resolved injectant visualizations which depend upon the magnitude of the coolant Strouhal number, St_c: (i) quasi-steady; and (ii) non-quasi-steady. St_c magnitudes less than 1–2 correspond to quasi-steady behavior, and St_c magnitudes greater than 1–2 correspond to non-quasi-steady behavior, regardless of the magnitude of the blowing ratio $\bar{m}$. With *quasi-steady film behavior*, the entire film concentration moves to and from the wall in a continuous stream so that the injectant distribution at each instant of time is the same as the steady distribution which would exist at the same instantaneous flow condition. Pulsation time periods ($1/2\pi n$) are longer than the time required for a parcel of injectant to pass into and out of a film cooling hole ($l/\bar{u}_c$). With *non-quasi-steady film behavior*, multiple pulsations are imposed on the injectant over the time period required for it to pass through a film hole ($1/2\pi n < l/\bar{u}_c$). As a result, portions of the film oscillate in ways different from adjacent portions, which gives a 'wavy' appearance at each instant in time such that larger injectant accumulations are spaced the distance that the film moves over one pulsation cycle. Because non-quasi-steady films show the largest alterations of time-averaged temperature (and injectant) compared to films with no pulsations, they are also expected to produce the most significant changes to surface film effectiveness distributions.

REFERENCES

1. A. B. Mehendale, J.-C. Han, S. Ou and C. P. Lee, Unsteady wake over a linear turbine cascade with air and CO_2 film injection: Part II—effect on film effectiveness and heat transfer distributions, *ASME Trans. J. Turbomach.* **116,** 730–737 (1994).
2. S. Ou, J.-C. Han, A. B. Mehendale and C. P. Lee, Unsteady wake over a linear turbine cascade with air and CO_2 film injection: Part I—effect on heat transfer coefficients, *ASME Trans. J. Turbomach.* **116,** 721–729 (1994).
3. S. Ou and J.-C. Han, Unsteady wake effect on film effectiveness and heat transfer coefficient from a turbine blade with one row of air and CO_2 film injection, *ASME Trans. J. Heat Transfer* **116,** 921–928 (1994).
4. R. P. Dring, M. F. Blair and H. D. Joslyn, An experimental investigation of film cooling on a turbine rotor blade, *ASME Trans. J. Engng Power* **102,** 81–87 (1980).
5. K. Takeishi, S. Aoki, T. Sato and K. Tsukagoshi, Film cooling on a gas turbine rotor blade, ASME Paper 91-GT-279, *ASME International Gas Turbine and Aeroengine Congress and Exhibition*, Orlando, Florida (1991).
6. R. J. G. Norton, A. E. Forest, A. J. White, D. G. Henshaw, A. H. Epstein, D. L. Schultz and M. L. G. Oldfield, Turbine cooling system design, Volume I—technical report, Report WRDC-TR-89-2109, Aero Propulsion and Power Laboratory, Wright Research Development Center, Air Force System Command, Wright-Patterson Air Force Base, Ohio (1990).
7. M. J. Rigby, A. B. Johnson and M. L. G. Oldfield, Gas turbine rotor blade film cooling with and without simulated shock waves and wakes, ASME Paper 90-GT-78, *ASME International Gas Turbine and Aeroengine Congress and Exhibition*, Brussels, Belgium (1990).
8. R. S. Abhari, and A. H. Epstein, An experimental study of film cooling in a rotating transonic turbine, *ASME Trans. J. Turbomachin.* **116,** 63–70 (1994).
9. D. A. Ashworth, J. E. LaGraff, D. L. Schultz and K. J. Grindrod, Unsteady aerodynamics and heat transfer processes in a transonic turbine stage, *ASME Trans. J. Engng Gas Turbines Power* **107,** 1022–1030.
10. A. B. Johnson, M. J. Rigby, M. L. G. Oldfield, R. W. Ainsworth and M. J. Oliver, Surface heat transfer fluctuations on a turbine rotor blade due to upstream shock wave passing, *ASME Trans. J. Turbomachin.* **111,** 105–115 (1989).
11. R. S. Abhari, G. R. Guenette, A. H. Epstein and M. B. Giles, Comparison of time-resolved turbine rotor blade heat transfer measurements and numerical calculations, *ASME Trans. J. Turbomachin.* **114,** 818–827 (1992).
12. S. K. Karlsson, An unsteady turbulent boundary layer, *J. Fluid Mech.* **14,** 622–636 (1959).
13. K. Al-Asmi and I. P. Castro, Production of oscillatory flow in wind tunnels, *Experiments Fluids* **15,** 33–41 (1993)
14. D. J. Doorly and M. L. J. Oldfield, Simulation of the effects of shock wave passing on a turbine rotor blade, *ASME Trans. J. Engng Gas Turbines Power* **107,** 998–1006 (1985).
15. P. M. Ligrani and W. W. Williams, Effects of an embedded

vortex on injectant from a single film-cooling hole in a turbulent boundary layer, *ASME Trans. J. Turbomachin.* **112,** 428–436 (1990).
16. P. M. Ligrani, J. M. Wigle, S. Ciriello and S. W. Jackson, Film-cooling from holes with compound angle orientations: Part 1. results downstream of two staggered rows of holes with 3D spanwise spacing, *ASME Trans. J. Heat Transfer* **116,** 341–352 (1994).
17. P. M. Ligrani, R. Gong, J. M. Cuthrell and J. S. Lee, Bulk flow pulsations and film cooling—II. Flow structure and film effectiveness, *Int. J. Heat Mass Transfer* **39,** 2283–2292 (1996).
18. J. M. Cuthrell, A study of film cooling and bulk flow pulsations, M.S. thesis, Department of Mechanical Engineering, University of Utah (1995).